Smart Structures and Systems, Vol. 9, No. 3 (2012) 253-271
DOI: http://dx.doi.org/10.12989/sss.2012.9.3.253

Seismic damage detection of a reinforced concrete structure by finite element model updating

Eunjong Yu*[1] and Lan Chung[2]

[1]*Department of Architectural Engineering, Hanyang University, Seoul 133-791, Korea*
[2]*Department of Architectural Engineering, Dankook University, Yong-In 448-701, Korea*

(Received March 22, 2010, Revised January 27, 2012, Accepted February 27, 2012)

Abstract. Finite element (FE) model updating is a useful tool for global damage detection technique, which identifies the damage of the structure using measured vibration data. This paper presents the application of a finite element model updating method to detect the damage of a small-scale reinforced concrete building structure using measured acceleration data from shaking table tests. An iterative FE model updating strategy using the least-squares solution based on sensitivity of frequency response functions and natural frequencies was provided. In addition, a side constraint to mitigate numerical difficulties associated with ill-conditioning was described. The test structure was subjected to six El Centro 1942 ground motion histories with different Peak Ground Accelerations (PGA) ranging from 0.06 g to 0.5 g, and analytical models corresponding to each stage of the shaking were obtained using the model updating method. Flexural stiffness values of the structural members were chosen as the updating parameters. In model updating at each stage of shaking, the initial values of the parameter were set to those obtained from the previous stage. Severity of damage at each stage of shaking was determined from the change of the updated stiffness values. Results indicated that larger reductions in stiffness values occurred at the slab members than at the wall members, and this was consistent with the observed damage pattern of the test structure.

Keywords: finite element model updating; damage detection; structural health monitoring; vibration; frequency response function; ill-conditioning

1. Introduction

Damage of civil engineering structures including multistory buildings gradually increases during their service life because of temporary overloads such as strong earthquake and/or hostile environmental effects. The traditional way of assessing the damage of RC structures is either by visual inspection or use of nondestructive testing (NDT) techniques. The NDT techniques included acoustic or ultrasonic methods, or X-ray inspection. In these methods, the overall health of a structure is judged based on the locations of observed cracks, their intensity and patterns, or the measured permanent deformation of individual structural members. However, inspection work using such methods is generally time-consuming and very cumbersome because of the need to remove coverings (e.g., panels or ceiling) to access local structural members being inspected. Furthermore, although such local methods are often efficient in assessing the severity of damage, they are generally not adequate for identifying the location of damage. Thus, to decide the overall health of the structure, the inspection needs to

*Corresponding author, Professor, E-mail: eunjongyu@hanyang.ac.kr

be carried out thoroughly throughout the structure. On the other hand, damage detection based on global methods which use information about the dynamic characteristics collected from vibration measurements does not require direct access to the structural members and has an advantage of locating damage. Consequently, global methods, such as dynamics-based damage identification methods, attract the engineers' attention as an alternative to the local methods (Doebling *et al*. 1996).

The global methods are based on the fact that changes of structural properties, such as damage, in the members affect its dynamic properties (e.g., natural frequencies, mode shapes, modal damping ratios and frequency response functions) of the structural system in their own way. A popular way being employed to determine the relationship between the changes in a structural system and the changes in dynamic properties is using finite element (FE) model updating techniques (Cheng *et al*. 2009, Mordini *et al*. 2007, Teughels *et al.* 2002, Ren and Reock 2002, Doebling *et al.* 2002). The FE model updating is an analytical optimization procedure that obtains optimal FE model that represents observed behaviors of a structure by adjusting the system's properties (e.g., the stiffness, mass, and/or damping parameters) of the FE model. Hence, when updating parameters are selected in a way that they are directly related to the physical attributes of the structural members, the locations and severity of the damage can be obtained from the comparison of two FE models, each of which represents dynamic characteristics before and after the damage, respectively.

Mathematically, the model updating which determines the properties of a system using its responses is inherently an inverse problem. Thus, depending on the selection of updating parameters and the amount of information contained in the measurements, an accurate solution cannot be always guaranteed. Even if a solution is obtained, it may be physically inadmissible and extremely unstable with the choice of measurement samples. The major cause of such numerical instability or inaccuracy is ill-conditioning of the updating equations, which occurs when two or more updating parameters that have similar effects on the system's response are chosen and the measurements are disturbed by noise (Zhang *et al.* 2000, Friswell and Mottershead 1995). For highly indeterminate structures such as building structures, the number of unknown parameters, such as the stiffness of structural members, is much greater than the number of measurements (these measurements are typically story accelerations), and some of the parameters may have similar effects on the response of the structure. Inevitably, parameters of such structures identified by model updating using limited measurements are very susceptible to ill-conditioning.

One way to address such numerical difficulty is using priori information. In this approach, referred to as the regularization method, the initial guess is carefully selected by engineering judgment, and the variation of parameters from the initial values is appended in the objective function. Thus, a set of parameters which sufficiently decreases the residuals (i.e., the differences between the measured and analytical response) with small changes from the initial values is selected as optimal values. Consequently, the solutions considerably depend on the initial guess of the updating parameters and the regularization factor which is for proportioning between the parameter change and residuals (Tikhonov and Arsenin 1977). The *L*-curve method (Hansen and O'Leary 1993) is one of the solution schemes to determine the optimal regularization factor.

Another approach to avoid the numerical difficulty is decreasing the number of parameters so that the possibility of ill-conditioning can be reduced. In this approach, it is important not to choose multiple parameters that have similar effects on the responses of the model; otherwise, it would result in ill-conditioning even though the number of updating parameters was sufficiently small. However, determining specific parameters among the potential candidates is not usually simple for large and complicated structures. Besides, when too small number of parameters is selected, it becomes

difficult to make plausible physical explanations to their updates because the remaining parameters more or less affect the system response as well.

Recently, to address this issue, an iterative FE model updating method by grouping the parameters was proposed (Yu *et al*. 2007a). In this method, constraints were imposed to any pair of parameters that have similar effects on the model response so that such parameters have similar values to each other. This strategy has the advantage of reducing the degree of ill-conditioning in the results while keeping the large set of parameters. This method was applied to detect preexisting damage of a four-story reinforced concrete building using measured data from forced vibration tests with a linear shaker mounted on top of the building. (Yu *et al*. 2008) The locations of the damage were determined from the comparison of updating results with carefully constructed analytical model. (Yu *et al*. 2007b) Determined locations of damage generally agreed with the observed locations of cracks in the building; however, it can be said that the reliability of the damage detection using the model updating method was not fully tested since damage detection in this example was carried out for one single damage state and the reference model (undamaged model) was taken from structural analysis.

In this paper, detection of location as well as the severity of the damage of a small-scale reinforced concrete structure was attempted using measured results from the shaking table test and the model-updating method with some modifications. During the test, the structure was subjected to a series of earthquake-type base excitations with increasing excitation amplitudes that caused increasing damage to the structure. Model updating for the structure was performed to detect damage at each stage of the test. Transfer functions and natural frequencies obtained from acceleration measurements at each floor and given ground acceleration history were used as the input for model-updating, and flexural stiffness of walls and slabs at each floor were determined. Subsequently, damage was identified from the comparison of updated stiffness of the members with the result of the previous stage. The following sections describe the details of the shaking table tests, summary of the model updating procedure, and model updating results applied to the test structure.

2. Shaking table test

2.1 Details of test

The test structure was a one-bay, five-story, reinforced-concrete wall-slab building. The dimensions of the members were scaled down to 1/5 of the typical member size of actual wall-slab type buildings. The story height and bay length of the test structure were 520 mm and 660 mm, respectively. The thickness of left wall, right wall, and slabs were 40 mm, 35 mm, and 30 mm, respectively, and the width of all members was 300 mm. The size and spacing of reinforcements for the members are indicated in Fig. 1. The diameter of deformed bars and coarse aggregate in reinforced concrete were reduced by the geometric scale factor. In addition, mass blocks were attached to the walls and the slabs to adjust the natural frequencies to $1/\sqrt{5}$ of the prototype structure to maintain an identical stress and strain relationship between the prototype structure and the scaled model. A yield strength of 368.64 MPa and a compressive strength of 26.67 MPa were obtained from the material tests of the deformed bar and the concrete, respectively.

The shaking table tests were performed on a uni-axial earthquake simulator. Inertia force was applied in the weak direction of the test structure, that is, in the out-of-plane direction of the walls. Accelerations and displacements at the base and each floor of the test structure were measured

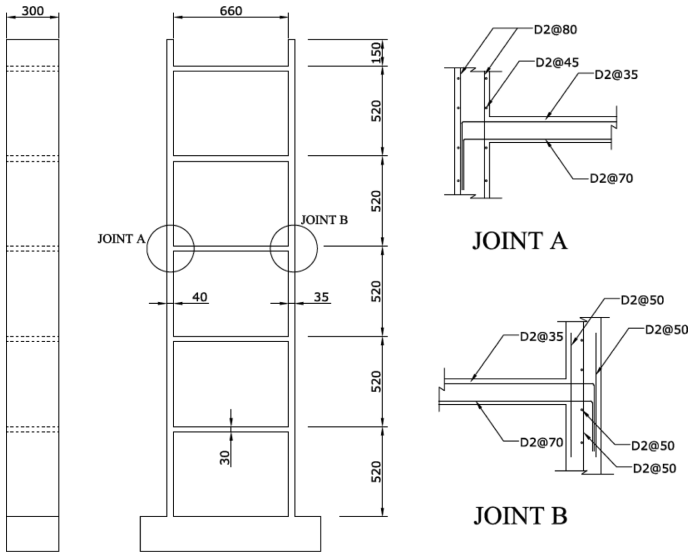

Fig. 1 Test structure

Table 1 Test sequence

	Test stage	Actual peak ground acceleration	Actual peak ground displacement
1	El Centro NS 1942 PGA=0.06 g	0.064 g	3.94 mm
2	El Centro NS 1942 PGA=0.12 g	0.098 g	6.02 mm
3	El Centro NS 1942 PGA=0.20 g	0.195 g	12.19 mm
4	El Centro NS 1942 PGA=0.30 g	0.317 g	20.19 mm
5	El Centro NS 1942 PGA=0.40 g	0.360 g	22.58 mm
6	El Centro NS 1942 PGA=0.50 g	0.476 g	37.37 mm

using accelerometers and LVDT's, respectively. The data were collected at a sampling frequency of 500 Hz. Overall test sequence consists of six El Centro earthquake tests with different Peak Ground Accelerations (PGA) ranging from 0.06 g to 0.5 g, as shown in Table 1. Actual peak acceleration and displacement at the base measured during the tests were also indicated. The time scale of the ground acceleration history for the test (El Centro NS, 1942) was scaled down by $1/\sqrt{5}$.

After each stage of the test, cracks of the structure were inspected and recorded. With the increase of the ground acceleration amplitude, some members of the test structure suffered significant damage from concentrated cracks at the end of the members. Fig. 2 shows the damage of the test structure observed at selected stages of the test. No noticeable cracks were observed until 0.12 g shaking. At 0.2 g shaking, the first major crack occurred at the right end of the third-floor slab (Fig. 2(b)) and minor cracks were observed at the base of the first-story wall on the right side. After the 0.3 g shaking, cracks were observed at the other side (i.e., at the left end) of the third-floor slab, both ends of the second-floor slab, and the right end of the fourth-floor slab. At 0.4 g shaking, no additional major cracks at new places were observed; however, the existing cracks especially at the slab ends significantly enlarged. Finally at 0.5 g shaking, new crack at the base of the first story wall on the left side was observed. During each test stage, lateral displacement of each floor was

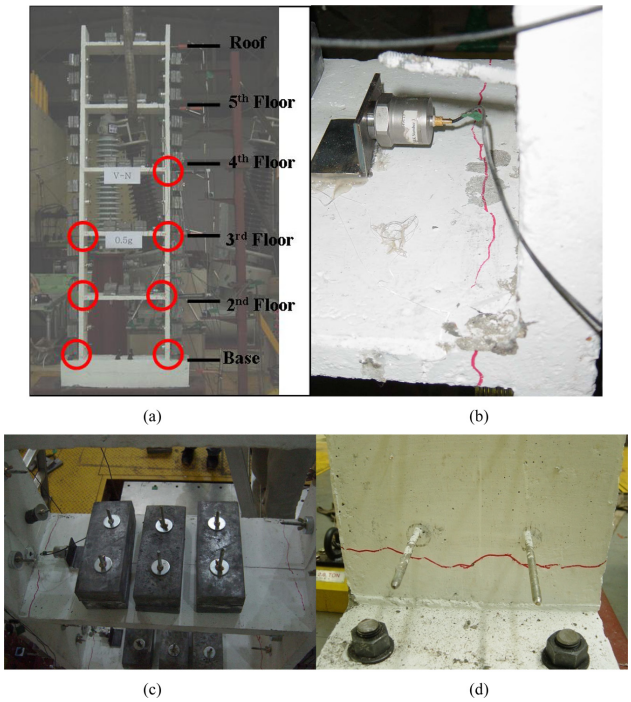

Fig. 2 Crack pattern observed after each stage of the El Centro ground acceleration tests: (a) location of observed cracks, (b) the right end of the third-floor slab, after 0.20 g shaking (c) the third and second-floor slab, after 0.30 g shaking and (d) the base of the first-story wall, after 0.50 g shaking

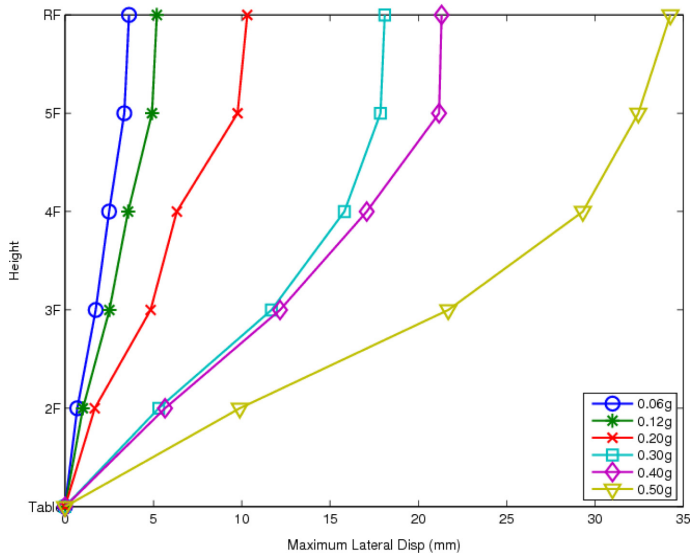

Fig. 3 Maximum lateral displacement at each stage of shaking

measured using LVDT's. Fig. 3 is the maximum lateral displacement profiles at each level of shaking. As shown in the figure, the lateral displacement at lower story was considerably increased with the increase of shaking intensity probably due to occurrence and development of cracks.

2.2 Modal identification

Modal properties such as the natural frequencies, damping ratios and mode shapes at each stage of shaking were determined from the measured acceleration data using system identification analyses. The system identification technique used in this research is the N4SID (subspace state-space system identification) (Overschee and DeMoor 1996), which is a type of time domain methods. The N4SID extracts the optimal state-space model from the input (base excitation) and output (acceleration response at each floor slab) of the system, and the modal properties are derived from the state-space model. However, due to measurement noise and numerical round-off error, some of the identified modes may not represent the physical properties of the structure. To distinguish these spurious modes from the structural (physical) modes, a stability plot indicating variations of identified natural frequencies, damping ratios, and mode shapes with the change of the order of the state-space model, was employed. Fig. 4 is the stability plot for the 0.12 g shaking, which indicates all identified modes as well as the stable modes, when the order of the state-space model is increased from 8 to 24. In this research, a stable mode is chosen as the mode satisfying the following conditions: the difference in results between the current and prior model should be (1) less than 1.5% for natural

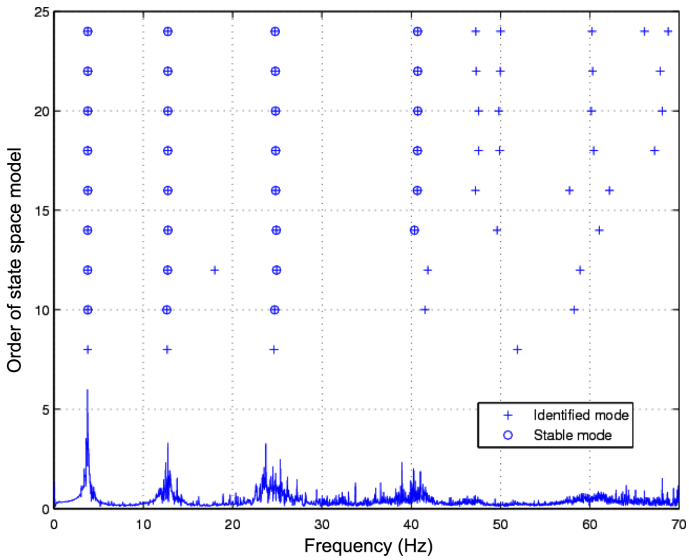

Fig. 4 Example of stability plot (0.12 g shaking)

Table 2 Identified natural frequencies and modal damping ratios

	Natural frequencies (Hz)				Damping ratios (%)			
	1st	2nd	3rd	4th	1st	2nd	3rd	4th
El Centro 0.06 g	4.01	13.08	25.15	41.60	2.56	2.78	3.87	5.68
El Centro 0.12 g	3.78	12.65	24.85	40.80	3.60	3.42	3.88	6.51
El Centro 0.20 g	3.00	11.06	22.42	39.73	10.43	5.19	7.20	11.16
El Centro 0.30 g	1.90	8.49	19.64	34.67	16.00	7.09	4.89	10.17
El Centro 0.40 g	1.59	8.16	18.55	33.40	15.90	5.72	5.30	10.83
El Centro 0.50 g	1.24	7.57	17.49	32.32	30.99	7.80	5.59	9.65

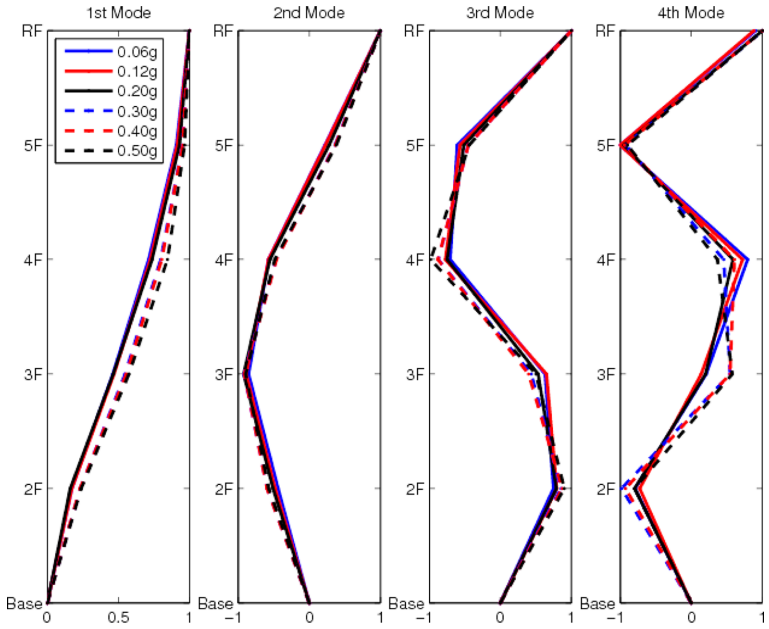

Fig. 5 Identified mode shapes

frequency, (2) less than 5% for damping ratio, and (3) more than 98% for the Modal Assurance Criterion (MAC) (Allemang and Brown 1982). The MAC value, defined by Eq. (1), is a metric of similarity between two mode shape vectors.

$$\mathrm{MAC}(\phi_A, \phi_B) = \frac{\{\phi_A^T \cdot \phi_B\}^2}{\{\phi_A^T \cdot \phi_A\}\{\phi_B^T \cdot \phi_B\}} \tag{1}$$

The natural frequencies and damping ratios for each stage of the El Centro earthquake tests identified through the procedure stated above were summarized in Table 2. As indicated in the table, modal properties up to the fourth mode could be identified. With the increase of vibration amplitude, the fundamental natural frequency gradually decreased and finally reached about 40% of that from the initial El Centro test. The damping ratio of the fundamental mode at the 0.5 g shaking was increased by about six times from the initial test, which is believed to be the result of hysteretic damping due to the nonlinear behavior of the test structure.

Fig. 5 represents the mode shapes of identified modes. As shown in the figure, the mode shapes from the three larger excitations, 0.30 g, 0.40 g, and 0.50 g, look similar to each other, but show some discrepancy with those from the three smaller excitations, 0.06 g, 0.12 g and 0.20 g. This indicates that the change of the overall stiffness distribution occurred somewhat abruptly during the 0.30 g shaking.

3. Summary of FE model updating procedure

FE model updating is an analytical procedure to obtain an optimal set of parameters of the numerical model by minimizing the differences between the response quantities from the experiment and the numerical model. Modal properties, such as the natural frequencies and the mode shapes, are the

most widely used response quantities to be matched in model updating. However, in reality, *all* modes of the structure can hardly be used for updating because extraction of modal properties of the complete modes is difficult. Even if they were obtained, they may possess large uncertainties, especially in the mode shapes. The lack of modal properties in higher modes may cause under-determinacy (rank deficiency) and ill-conditioning of the updating equations, and thus produce unreliable updating results. To alleviate these potential problems in this study, frequency response functions (FRF) were used for updating in addition to the natural frequencies. By including the FRF, more accurate information about the higher mode behavior can be supplied and, at the same time, an over-determinate updating equation can be obtained. The updating procedure adopted in this study basically solves the nonlinear optimization problem by the iterative least-squares equation based on sensitivity matrix and residual vector, appended by the side constraints to ensure stable solutions.

3.1 Sensitivity matrices

3.1.1 FRF-based sensitivity

The equation of motions of the system with n degrees-of-freedom subjected to base accelerations $\ddot{u}_g$

$$\boldsymbol{M}\ddot{u}(t) + \boldsymbol{C}\dot{u}(t) + \boldsymbol{K}u(t) = -\boldsymbol{M}\boldsymbol{L}\ddot{u}_g(t) \tag{2}$$

can be converted into the frequency domain, as in Eq. (3), using the dynamic stiffness matrix $\mathbf{B}(\omega)$ and the transfer function vector, $\boldsymbol{H}(\omega)$.

$$\boldsymbol{B}(\omega)\boldsymbol{H}(\omega) = -\boldsymbol{L} \tag{3}$$

where

$$\boldsymbol{B}(\omega) = \boldsymbol{M}^{-1}(-\mathbf{M}\omega^2 + i\boldsymbol{C}\omega + \boldsymbol{K}), \text{ and} \tag{4}$$

$$\boldsymbol{H}(\omega) = \frac{u(\omega)}{\ddot{u}_g(\omega)} \tag{5}$$

Here, $\boldsymbol{M}$, $\boldsymbol{C}$ and, $\boldsymbol{K}$ are ($n\times n$) mass, damping and stiffness matrices of the system, respectively. $\boldsymbol{H}(\omega)$ is the transfer function vector defined by the ratio of ($n\times 1$) relative story displacement vector $\boldsymbol{u}(\omega)$ to base acceleration $\ddot{u}_g(\omega)$, and $\boldsymbol{L}$ is the influence vector indicating the location of DOFs being excited by $\ddot{u}_g(\omega)$.

For updating, the transfer function $\boldsymbol{H}(\omega)$ is replaced with $\tilde{\boldsymbol{H}}(\omega)$ that is obtained from measured base acceleration $\ddot{u}_g(\omega)$ and measured absolute story acceleration $\ddot{\boldsymbol{u}}_t(\omega)$ using Eq. (6).

$$\boldsymbol{H}(\omega) = \frac{\boldsymbol{u}(\omega)}{\ddot{u}_g(\omega)} = -\frac{1}{\omega^2}\left(\frac{\ddot{\boldsymbol{u}}_t(\omega)}{\ddot{u}_g(\omega)} - \boldsymbol{l}\right) \tag{6}$$

In addition, the dynamic stiffness matrix $\boldsymbol{B}(\omega)$ is replaced by the analytical counterpart $\boldsymbol{B}(\boldsymbol{p},\omega)$, which is an explicit function of a set of updating parameters, $\boldsymbol{p}=[p_1, p_2,..., p_m]^T$, that are used in constructing the structural matrices $\boldsymbol{M}$, $\boldsymbol{C}$, and $\boldsymbol{K}$ through a FE model. As such, an optimal parameter vector is one that minimizes the objective functions in Eq. (7), which is the Euclidean norm of the error vector.

$$\left\|\boldsymbol{e}_F(\boldsymbol{p})\right\|^2 = \left\|l + \boldsymbol{B}(\boldsymbol{p}, \omega)\tilde{\boldsymbol{H}}(\omega)\right\|^2 \tag{7}$$

As mentioned above, the objective function is generally nonlinear with respect to the updating parameters, the equations are first linearized using the Taylor series expansion up to the first order, and the solution is obtained using an iterative calculation such as the Newton's method. By the Taylor series expansion about the parameter vector at the current iteration $\boldsymbol{p}_k$, $\boldsymbol{B}(\boldsymbol{p},\omega)$ is approximated as

$$\boldsymbol{B}(\boldsymbol{p}, \omega) \approx \boldsymbol{B}(\boldsymbol{p}_k, \omega) + \sum_{i=1}^{m} \Delta p_i \frac{\partial \boldsymbol{B}(\boldsymbol{p}_k, \omega)}{\partial p_i} = \boldsymbol{B}(\boldsymbol{p}_k, \omega) + \boldsymbol{B}_{,1}(\boldsymbol{p}_k, \omega)\Delta p_1 + \cdots + \boldsymbol{B}_{,m}(\boldsymbol{p}_k, \omega)\Delta p_m \quad (8)$$

where

$$\boldsymbol{B}_{,i}(\boldsymbol{p}_k, \omega) = \frac{\partial \boldsymbol{B}(\boldsymbol{p}_k, \omega)}{\partial p_i} \quad (9)$$

indicates the gradient of $\boldsymbol{B}(\boldsymbol{p},\omega)$ at the current parameter vector $\boldsymbol{p}_k$ with respect to the i-th parameter over the frequency range $\omega = [\omega_1, \omega_2, \ldots, \omega_s]$. Substituting Eq. (8) into Eq. (7), and setting the norm of the error vector to zero, we get

$$\sum_{i=1}^{m} \boldsymbol{B}_{,i}(\boldsymbol{p}_k, \omega)\tilde{\boldsymbol{H}}(\omega)\Delta p_i = l + \boldsymbol{B}(\boldsymbol{p}_k, \omega)\tilde{\boldsymbol{H}}(\omega) \quad (10)$$

Eq. (10) can be rewritten as a sensitivity matrix and a residual vector form as in Eq. (11).

$$\mathbf{S}_k^F \Delta \mathbf{p}_k = \mathbf{r}_k^F \quad (11)$$

3.1.2 Natural frequency sensitivity

The sensitivity matrix based on the natural frequency can be obtained in a similar manner. The j-th component of error vector (i.e., the relative difference between the j-th mode natural frequencies from measured data λ_j and the analytical natural frequency $\lambda_j(\boldsymbol{p})$) can be expressed as Eq. (12), and the equation of the gradient of $\lambda_j(\boldsymbol{p})$ and the residual at the current parameter vector $\boldsymbol{p}_k$ obtained by the Taylor series expansion is expressed as Eq. (13).

$$e_j^M = \frac{\lambda_j(\boldsymbol{p}) - \tilde{\lambda}_j}{\tilde{\lambda}_j} \quad (12)$$

$$\sum_{i=1}^{m} \lambda_{,i}(\boldsymbol{p}_k)\Delta p_i = \frac{\lambda_j(\boldsymbol{p}_k) - \tilde{\lambda}_j}{\tilde{\lambda}_j} \quad (13)$$

Similar to Eq. (11), updating equation with respect to the natural frequency can be written using the sensitivity matrix $\boldsymbol{S}_M$ and the residual vector $\boldsymbol{r}_M$ as

$$\boldsymbol{S}_k^M \Delta \boldsymbol{p}_k = \boldsymbol{r}_k^F \quad (14)$$

Because it is not generally possible to identify the natural frequencies of all modes accurately from measured data, the analytical natural frequency vector is truncated to contain the counterparts of the experimental natural frequencies that were determined with confidence.

3.2 Weightings and constraints

Combining Eqs. (11) and (14), the incremental sensitivity equations based on FRF and the natural frequency, we have

$$\boldsymbol{S}_k \Delta \boldsymbol{p}_k = \boldsymbol{r}_k \tag{15}$$

where the combined sensitivity matrix $\mathbf{S}_k$, and the residual vector $\mathbf{r}_k$ are defined as

$$\boldsymbol{S}_k \equiv \begin{bmatrix} \mathrm{Re}(\boldsymbol{S}_k^F) \\ \mathrm{Im}(\boldsymbol{S}_k^F) \\ \boldsymbol{S}_k^F \end{bmatrix}, \boldsymbol{r}_k \equiv \begin{Bmatrix} \mathrm{Re}(\boldsymbol{r}_k^F) \\ \mathrm{Im}(\boldsymbol{r}_k^F) \\ \boldsymbol{r}_k^M \end{Bmatrix} \tag{16}$$

Note that the real and imaginary parts in Eq. (16) are separated.

The relative contributions between the two types of response quantities (e.g., FRF and natural frequency, respectively) can be adjusted using a weighting matrix. Since the sensitivity terms from the FRF data occupy a vast majority of the elements of the sensitivity matrix, larger weighting factors should typically be assigned to the modal data. The weighted version of Eq. (15) is

$$\boldsymbol{S}_k^T \boldsymbol{W} \boldsymbol{S}_k \Delta \boldsymbol{p}_k = \boldsymbol{S}_k^T \boldsymbol{W} \boldsymbol{r}_k \tag{17}$$

where $\boldsymbol{W}$ is a diagonal matrix containing the weighting factors. From the statistical theory, the best weighting matrix for the least-squares problem is known as the inverse of the covariance matrix of the measurement uncertainty (Friswell and Mottershead 1995). However, this information is generally not available in most cases, the weighting factors are usually chosen by engineering judgement considering presumed importance of each measurement and the amount of noise contained.

As mentioned earlier, the conventional least-squares solution produces big changes in a few parameters from their initial values to ill-conditioned model-updating problems. Such ill-conditioning occurs when two or more parameters have very similar effect on the response of the system and the measurements are contaminated by noise. Accordingly, the sensitivity vectors associated with the similar parameters are very close to collinear vectors, thus a small change in the sensitivity vectors caused by noise causes a big change in their intersection point (i.e., the solution of the equation). Consequently, the obtained parameters from the ill-conditioned updating problem have large variations, sometimes updated stiffness or mass parameters may results in negative values which cannot be explained in a physical sense. Theoretically, to avoid this problem, a sufficiently small number of parameters that have independent sensitivity vectors (i.e., with sufficiently large angles between their sensitivity vectors) should be chosen. However, selection of appropriate parameters from the candidates is not straightforward in the case of complex and large structures. In addition, elimination of too many parameters may not be adequate since unselected parameters also contribute to the system's response, thus, assumed values for them would affect the updating results.

The strategy adopted in this paper to address this issue is grouping of updating parameters similar to Yu *et al*. (2007a). In this method, any pair of parameters that have similar effects on the model response are grouped so that such parameters have similar values to each other. Since the columns of the sensitivity matrix can be considered as vectors in multidimensional space, similarity between the sensitivity vectors can be examined in terms of the cosine angle as Eq. (18).

$$\text{angle}(\boldsymbol{S}_i, \boldsymbol{S}_j) = \frac{\{\boldsymbol{S}_i^T \cdot \boldsymbol{S}_j\}}{\sqrt{\{\boldsymbol{S}_i^T \cdot \boldsymbol{S}_i\}}\sqrt{\{\boldsymbol{S}_j^T \cdot \boldsymbol{S}_j\}}} \tag{18}$$

where $\boldsymbol{S}_i$ and $\boldsymbol{S}_j$ are the sensitivity vectors (i.e., the i-th and j-th columns of the sensitivity matrix $\boldsymbol{S}$) with respect to the updating parameters p_i and p_j, respectively. The term angle ($\boldsymbol{S}_i$, $\boldsymbol{S}_j$) denotes the cosine angle between the vectors $\boldsymbol{S}_i$ and $\boldsymbol{S}_j$, having a value ranging from zero to one. Actually, Eq. (18) is identical to the square root of the value given by Eq. (1) that has been used to examine the similarity between two mode shape vectors.

Then, constraints that restrict the deviation of two parameters that have similar effects on the system response are given to the updating equation. That is

$$|p_i - p_j| < 1 - \text{angle}(\boldsymbol{S}_i, \boldsymbol{S}_j), \quad \text{if} \quad \text{angle}(\boldsymbol{S}_i, \boldsymbol{S}_j) > c_{lim} \tag{19}$$

Eq. (19) represents the constraints placed on the relative variations between *any* two parameters. If two parameters have similar effects on the response (e.g., the angle between the two sensitivity vectors is larger than a given limit c_{lim}), then the difference between the two updated parameters is restricted to remain within a range that depends on their degree of similarity. This requirement forces the updating parameters to change similarly (between iterations) if they have similar effects on the structural response. Because similar parameters are actually interconnected to each other, this method has the effect of reducing the actual number of parameters while keeping a large set of parameters. In the original proposal of this method (Yu *et al*. 2007a), a correlation coefficient of the sensitivity vectors was used in place of Eq. (18). When the sensitivity vectors are zero-mean vectors, both of the value by the correlation coefficient and the cosine angle give identical values. However, sensitivity vectors would not always be zero-mean vectors. Therefore, the use of the cosine direction rather than the correlation coefficient is more appropriate to compare the influence of parameters on the system's response.

Comparisons of sensitivity vectors in terms of the cosine angle were also introduced in Shahverdi (2006). For updating of the analytical model for the tailcone of a helicopter, they built a sensitivity matrix based on natural frequency and mode shapes with respect to a large set of parameter candidates, and then used the cosine angle to examine the similarity of the parameters. However, they used this information to reduce the number of updating parameters by assigning single parameter to similar parameters of the original parameter set, and did not allow difference between them.

The least-squares solution of Eq. (17), subject to the constraints provided in Eq. (19), can be achieved using the standard Bounded Variables Least Squares (BVLS) technique (Stark and Parker 1995). Parameter vector $\boldsymbol{p}$ is updated by Eq. (20), and iteration continues until convergence is achieved (i.e., when the residual norm falls below a properly chosen tolerance value).

$$\boldsymbol{p}_{k+1} = \boldsymbol{p}_k + \Delta\boldsymbol{p}_k \tag{20}$$

4. Model updating of the test structure

4.1 Initial model

The initial analytical model for the test structure was constructed based on the information obtained from the member dimension and material test results. Conventional assumptions for building structures

were used in constructing the FE model. That is, (i) building masses are lumped at the floor levels; (ii) floor diaphragms are rigid in-plane, but are flexible in out-of-plane directions; and (iii) damping is classical (mode-proportional). Young's modulus for concrete was evaluated from the compressive strength of core sample tests using the equation in ACI 318 (2005)

$$E_c = 4700\sqrt{f_c'} \tag{21}$$

Obtained average Young's modulus of concrete was 24.77 GPa. Stiffness of the members of the initial model was determined based on the moment of inertia of a gross (uncracked) section. Story mass was obtained from the self weight of the members and mass blocks attached to the test structure with values of 108.87 kg for the roof floor, and 138.08 kg for other floors. The resulting natural frequencies of the initial FE model were 3.63, 11.92, 22.76, 35.89, and 47.74 Hz for the first to fifth modes, respectively.

Effective flexural stiffness factors (i.e. the ratio of actual flexural stiffness to the initial one) of the structural members were chosen as the updating parameter since these values will change with the progress of cracking. Initially, sensitivity vectors of all members (10 walls and 5 slabs) were obtained and their similarities in terms of the cosine angle between the sensitivity vectors of their respective members using Eq. (18) were investigated. The results indicated that the effects of the two wall members in one story were almost identical to each other (the cosine angles of the five pairs of the members were 97% ~ 99.9%). The two wall members in a story were represented using a single parameter. As a result, a total of 10 parameters that consist of the factors for five wall groups and five slabs were defined as shown in Fig. 6. The optimal values for parameters were obtained by the model updating equation of Eq. (17) considering the constraints of Eq. (19). At each iteration, values

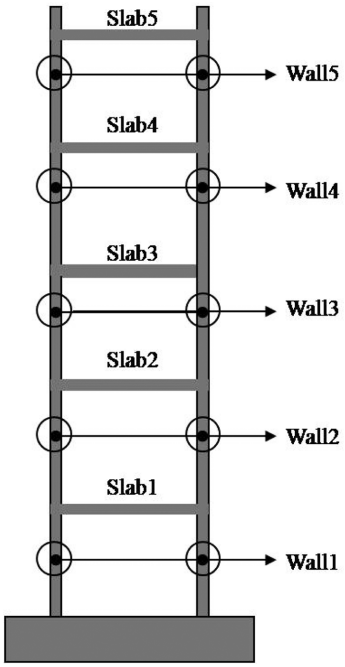

Fig. 6 Assignment of updating parameters

of 1.5 and 0.05 were given for upper and lower bounds, respectively. The limit in Eq. (19) was given as 0.65 in this study. For the updating of each stage of shaking, transfer functions were evaluated at 100 points between 1.0 Hz and 50 Hz with an increment of 0.4883 Hz, and the natural frequencies of first - fourth mode obtained from the system identification were used. A weighting factor of 100 was used for the sensitivity matrix and residual vector associated with the modal data, while the weighting factor for FRF was taken as unity. Such weighting factors were chosen by engineering judgement considering that the size of sensitivity matrix from the FRF data was 50 times larger than that from the modal data, and that the modal data would be more accurate than the FRF data which inherently contains leakage errors.

Damping ratios for that stage obtained from system identification were assigned to the initial model, and the damping ratios and story mass were not altered throughout the updating. A damping ratio of 5% was assigned to the fifth mode, which had not been obtained from system identification.

A Matlab (Mathworks 2009) code generating the condensed stiffness matrix for the test structure was implemented, and the sensitivity matrix was evaluated numerically using the rates of change of the responses (i.e., FRF and natural frequency) to small perturbations of the updating parameters. For the first stage of the test (PGA=0.06 g), the initial values of all parameters were set to 1.0. However, for the rest of the test stage, updated parameter values from the previous test stage were used as the initial values.

4.2 Updated model and damage detection

Fig. 7 displays the convergence plots for the 0.20 g shaking, which shows the change of the norm of parameter update vector ($\Delta \boldsymbol{p}$) as well as the norm of the residual vector ($\mathbf{r}$) during the iterative solution process. Iterations were terminated when the parameters were stabilized (when the norm of

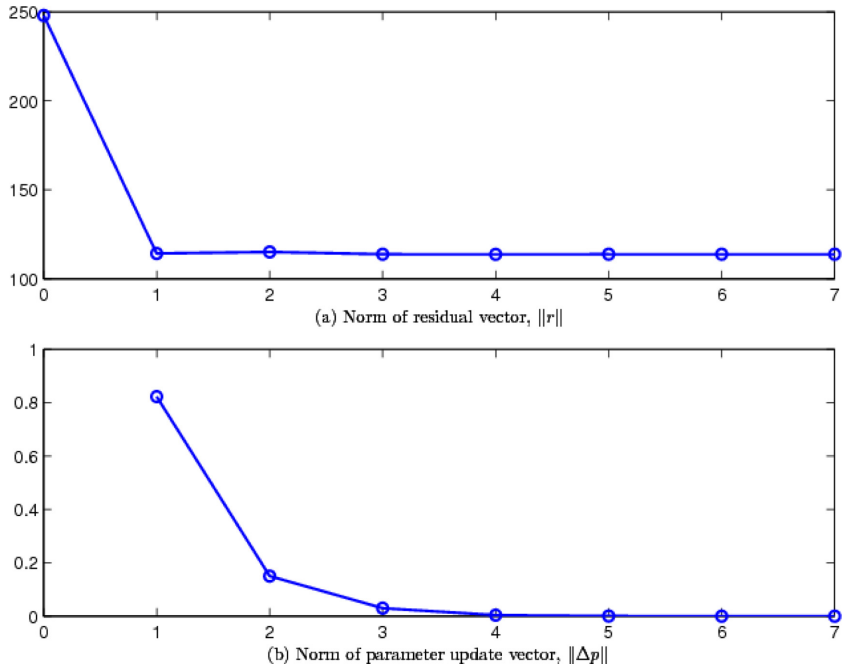

Fig. 7 Example of convergence plot (at the 0.20 g shaking)

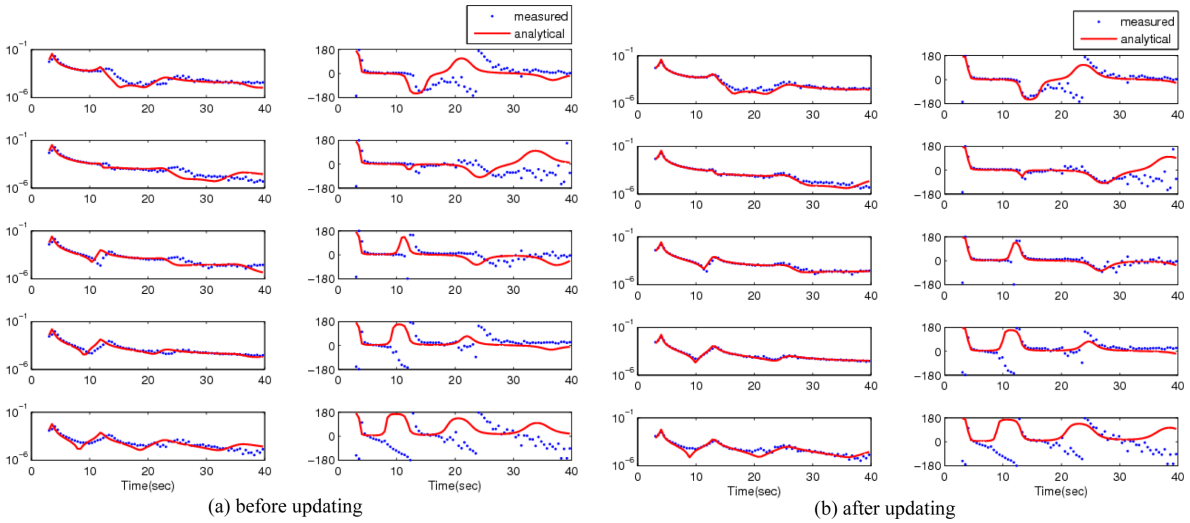

(a) before updating (b) after updating

Fig. 8 Comparison of analytical and measured FRF's before and after the updating (PGA=0.20 g) (left: amplitude, right: phase angle)

the parameter update vector, $\|\Delta \boldsymbol{p}\|$, became less than 0.1%). Fig. 8 compares the analytical and measured FRF before and after the updating for PGA=0.20 g. Comparisons of FRF at other stages showed similar fashion, however, as the increase of excitation level the match of FRF curve after updating gets worse probably due to nonlinear behavior of the test structure. In Fig. 8, the figures on the left side shows the amplitude of the measured and analytical FRFs plotted in log scale, while the figures on the right side compares the phase angles in degree. Although the purpose of model updating is to minimize the differences in measured and analytical models, the measured and analytical FRF curves cannot be completely identical even after updating mainly due to the measurement noise,

Table 3 Comparison of natural frequencies between the measured and the updated models

		1st		2nd		3rd		4th	
		Freq. (Hz)	Percent error	Freq. (Hz)	Percent error	Freq. (Hz)	Percent error	Freq. (Hz)	Percent error
0.06 g	Measured	4.01	0%	13.08	0%	25.15	2%	41.60	-2%
	Updated	4.00		13.02		25.59		40.89	
0.12 g	Measured	3.78	0%	12.65	0%	24.85	1%	40.80	-2%
	Updated	3.78		12.68		24.99		40.13	
0.20 g	Measured	3.00	4%	11.06	1%	22.42	-1%	39.78	-7%
	Updated	3.13		11.17		22.14		36.00	
0.30 g	Measured	1.90	6%	8.49	4%	19.64	-9%	34.67	-15%
	Updated	2.03		8.79		17.80		29.38	
0.40 g	Measured	1.59	14%	8.16	-1%	18.55	-13%	33.40	-21%
	Updated	1.82		8.04		16.10		26.45	
0.50 g	Measured	1.24	17%	7.57	-8%	17.49	-15%	32.32	-23%
	Updated	1.45		6.98		14.90		24.78	

especially in the frequency ranges around the anti-resonance frequencies. This is because the amplitudes of FRFs around the anti-resonance frequencies are low, and thus susceptible to measurement noise. On the other hand, the values of FRFs around the resonance frequencies are large and affects greatly on the error norm (i.e., sum of squared errors in both of real and imaginary parts of the FRFs and the natural frequency as in Eq. (16)). It can be seen that peak frequencies of measured and analytical FRFs did not match before updating, but after updating such mismatches were greatly reduced.

Table 3 shows the comparison of natural frequencies from the measured response and the updated model. When the excitation amplitude is small, natural frequencies of the updated model show an almost perfect match with the measured values. However, as the excitation amplitude increases, the natural frequencies of the updated model started to show some discrepancies, probably due to nonlinear behavior within the single set of measurement.

$$\text{Percent Error} = \frac{(\text{updated - measured})}{\text{measured}} \tag{22}$$

The effective flexural stiffness values (i.e., the updating parameter values) for each test stage obtained using the model updating procedure is summarized in Table 4 and Fig. 9. Values in Table 4 indicate the ratios of the member stiffnesses of updated model to those of the initial model. As mentioned before, the stiffness of the initial model was determined based on the moment of inertia of uncracked section and modulus of elasticity of concrete specified in ACI. The modulus of elasticity of concrete specified in ACI is based on the secant stiffness to the 45% of maximum strength from the origin in stress-strain curve (ACI 318 2005). Thus, when the excitation is small the slope is larger than the code-specified value; accordingly the effective flexural stiffness can be larger than the initial value. Effective stiffness at each stage in Table 4 were normalized by the first shaking (0.06 g) and presented in Table 5. Bold letters in the tables represent the locations at which cracks were observed. The overall distribution of effective flexural stiffness values indicated that the stiffness drop was more severe at the slab than at the wall. As indicated in the table, a big drop in the effective flexural stiffness values generally coincided with the crack's occurrence (i.e., slabs at the second, third, and forth floors after the 0.30 g shaking, and walls at the first story after the 0.30 g shaking). In the case of the fifth floor slab(Slab4), Table 4 shows considerable stiffness degradation, whereas no major cracks were observed from the visual inspection. The stiffness of Slab4 was continuously decreasing with the increase of shaking, finally reached to 17% of the first shaking. The degradation was not as severe as Slab1~Slab3, but larger than Wall1. The reason why Slab4 has larger stiffness degradation without major crack development in contrast with Wall1 is probably due to the difference in the reinforcement ratios.

Table 4 Updated effective stiffness values

	Wall					Slab				
	Wall1	Wall2	Wall3	Wall4	Wall5	Slab1	Slab2	Slab3	Slab4	Slab5
0.06 g	1.30	1.35	1.22	1.37	1.38	1.23	1.16	1.23	0.95	1.22
0.12 g	1.28	1.37	1.12	1.42	1.43	1.12	0.90	1.10	0.85	1.10
0.20 g	**1.07**	1.21	1.00	1.26	1.29	0.67	**0.46**	0.67	0.56	0.96
0.30 g	**0.68**	0.86	0.72	0.90	0.95	**0.27**	**0.15**	**0.28**	0.30	0.71
0.40 g	**0.59**	0.83	0.72	0.88	0.91	**0.17**	**0.08**	**0.18**	0.23	0.69
0.50 g	**0.46**	0.76	0.68	0.80	0.78	**0.09**	**0.04**	**0.10**	0.16	0.62

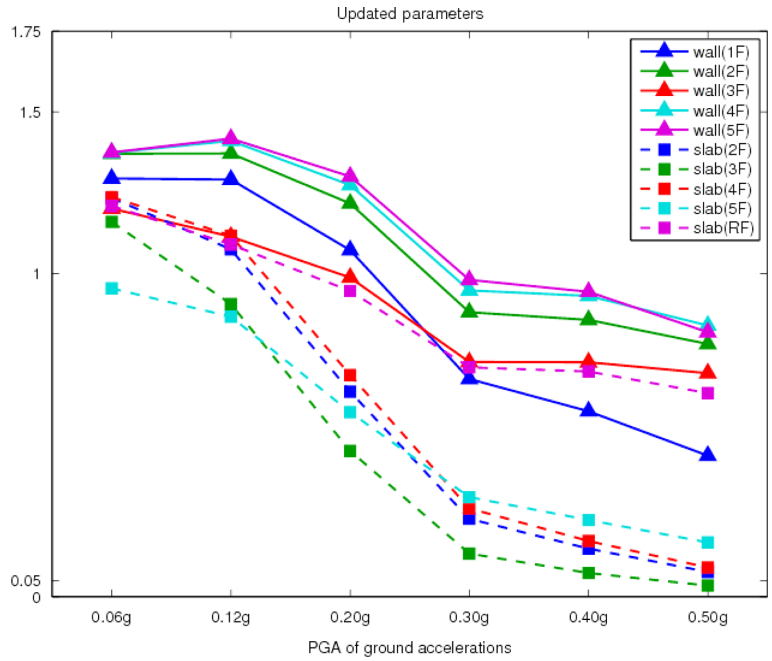

Fig. 9 Updated parameter values

Table 5 Ratio of updated effective stiffness values to the 0.06 g shaking

	Wall					Slab				
	Wall1	Wall2	Wall3	Wall4	Wall5	Slab1	Slab2	Slab3	Slab4	Slab5
0.06 g	100%	100%	100%	100%	100%	100%	100%	100%	100%	100%
0.12 g	98.5%	101%	91.8%	103%	103%	91.1%	77.6%	89.4%	89.5%	90.2%
0.20 g	**82.3%**	89.6%	82.0%	92.0%	93.5%	54.5%	**39.7%**	54.5%	58.9%	78.7%
0.30 g	**52.3%**	63.7%	59.0%	65.7%	68.8%	**22.0%**	**12.9%**	**22.8%**	31.6%	58.2%
0.40 g	**45.4%**	61.5%	59.0%	64.2%	65.9%	**13.8%**	**6.9%**	**14.6%**	24.2%	56.6%
0.50 g	**35.4%**	56.3%	55.7%	58.4%	56.5%	**7.3%**	**3.4%**	**8.1%**	16.8%	50.8%

Stiffness of a RC section is very sensitive to crack occurrence especially for the members which was very lightly reinforced as the slab members in this specimen (reinforcement ratio=0.3%) Section analysis of these slabs indicates that when the tension bars reach to the yield strain (i.e., at yield moment), the stiffness of the section was decreased to only 15% of the stiffness of the uncracked section. On the other hand, when the reinforcement ratio was increased to 1.2%, stiffness of the section at yield moment becomes almost 40% of that of uncracked section. This is seemingly the reason why the wall sections, which had larger reinforcement near the joint due to the splicing of vertical bars and embedment of slab bars, retained relatively high stiffness even after the occurrence of minor cracks. It is presumed that Slab4 reached close to yielding stage and tiny cracks were developed at the member ends. Actually, linear time history analysis using initial FE model (before updating of 0.06 g shaking) with obtained damping ratios at the 0.20 g shaking (in Table 2) and measured base accelerations at 0.20 g shaking showed that maximum moment at the end of Slab4 was in the range of 90%~123% of moment capacity of the section. Although the linear time history

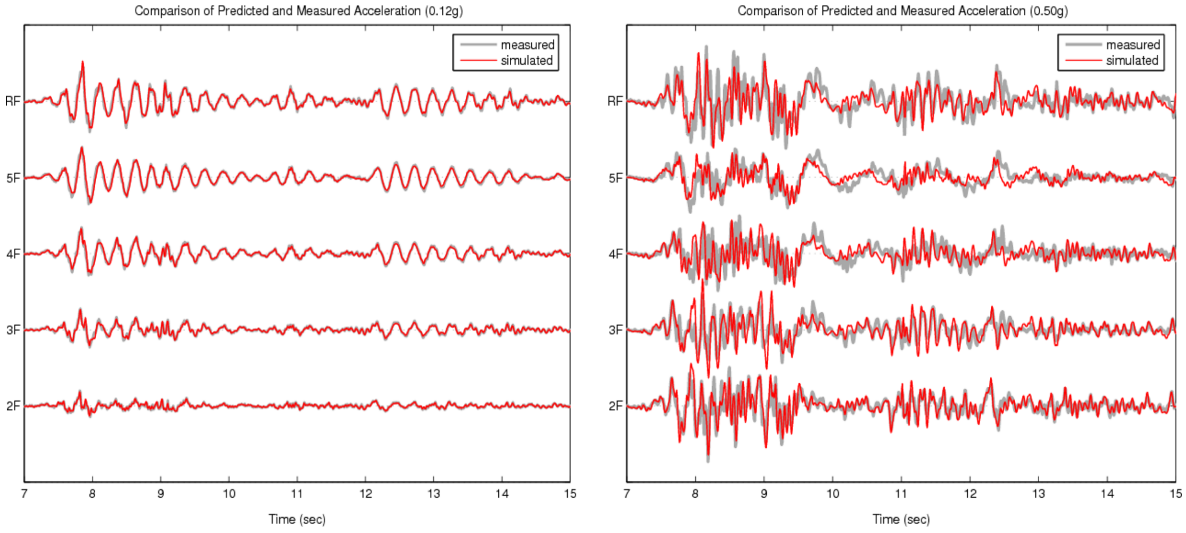

Fig. 10 Comparison of predicted and measured responses (a) 0.12 g shaking and (b) 0.50 g shaking

analysis is not accurate because stiffness degradation and moment redistribution cannot be considered, it seems quite probable that the developed moment at the ends of Slab4 exceeded or at least reached to the yield moment during the strong shakings.

As mentioned earlier, another approach to address the numerical difficulties associated with ill-conditioning is using the regularization method. Model updating by the regularization method using the procedure proposed by Hansen and O'Leary (1993) was attempted with the same sets of data. In the solutions by the regularization method, the values of some parameters changed to negative values in two or three iterations, and thus, overall solution failed to converge, probably due to large measurement noise contained in the dataset. On the other hand, model updating procedure proposed in this study (Table 4 and Fig. 9) shows consistent and reliable results; updated effective flexural stiffness never diverged, and kept decreasing with the increase of applied vibration amplitude although results for high excitation amplitude (e.g., 0.50 g shaking) may contain larger errors due to nonlinear behavior.

Predicted responses using the updated model and measured acceleration are compared in Fig. 10. As in the natural frequency comparison, at low level excitation, the predictions almost exactly replicated the measured responses. However, similar to the FRF and the natural frequencies comparisons, the accuracy of the predictions became worse with the increase of excitation level, due to large errors in parameter values (updated parameters), which may be inferred from Table 3. This would be inevitable limitation in identifying nonlinear behaviors with the linear model. For example, identified damping ratios at 0.50 g shaking were in the range of 5.59% ~ 30.99% as can be seen in Table 2. These values were used for the damping ratios of the linear model in updating of the 0.50 g shaking. However, hysteretic behaviors of the structure cannot be accurately simulated using a linear model with equivalent viscous damping. Another limitation can be inability of accounting for the hinge formulation. The structure behaves nonlinearly by formulating plastic hinges at the end of members. However, in the current model updating procedure, the effects of the plastic hinge (or degraded stiffness only at member ends) is accounted for just by decreasing the stiffness of the member along its entire length. These issues should be addressed in future studies.

5. Conclusions

Finite element (FE) model updating is a useful tool for global damage detection technique, which detects the damage of the structure from measured vibration data. In structural damage detection using the FE model updating the numerical stability is an important issue, since noises contained in experimentally measured data bring about physically inadmissible solutions. In this paper, damage of a 5-story reinforced concrete wall-slab structure subjected to earthquake-type ground excitations with various excitation amplitudes was identified using an improved sensitivity-based model updating procedure. The model updating strategy adopted in this paper is based on the nonlinear least-squares solution with a side constraint to mitigate numerical difficulties associated with ill-conditioning. The side constraint was established using the cosine angle which quantifies the similarity between the sensitivity vectors for the parameters to prevent unrealistic departure of parameter values, which typically occurs when the influences of two or more parameters on the system responses are similar. Transfer functions and natural frequencies obtained from acceleration measurement at each floor and given ground acceleration history were used as the input for model updating, and effective stiffness factors for five wall groups and five slabs at each stage of shaking were obtained. In model updating for each stage of shaking, the initial values of the parameter were set to those obtained from the previous stage.

The model updating procedure proposed in this study showed consistent and reliable results. Updated effective flexural stiffness never diverged and kept decreasing with the increase of applied vibration amplitude, whereas the solutions using the regularization method, which is another approach to address the ill-conditioning, failed to converge. In tracking the change of stiffness values of the members, it was observed that the drastic decrease of stiffness occurred during the 0.3 g shaking. With the increment of peak acceleration of excitation from 0.06 g to 0.50 g, updated stiffness decreased to 35% at most for wall members and to 3.4% for slab members. Although the dynamic responses of the updated model at large amplitude excitations were not as accurate as at low amplitude excitations due to nonlinear behaviors, overall distribution of stiffness indicated that damage was most severe in the slab members in the lower stories, which was generally consistent with the observed damage patterns of the test structure. Also, degradation of stiffness was more severe in the slab members than in the wall members, which is believed to be caused by the difference in the reinforcement ratios.

References

ACI Committee 318 (2005), *Building code requirements for structural concrete and commentary (ACI 318M-05); American Concrete Institute*, Farmington Hills, Michigan.

Allemang, R.J. and Brown, D.L. (1982), "A correlation coefficient for modal vector analysis", *Proceedings of the 1st International Modal Analysis Conference*, Orlando, Florida.

Cheng, L., Xie, H.C., Spencer, B.F. and Giles, R.K. (2009), "Optimized finite element model updating method for damage detection using limited sensor information", *Smart Struct. Syst*., **5**(6), 681-697.

Doebling, S.W., Farrar, C.R. and Prime, M.B. (1988), "A summary review of vibration-based damage identification methods", *Shock Vib*., **30**, 91-015.

Doebling, S.W., Farrar, C.R., Prime, M.B. and Shevitz, D.W. (1996), *Damage identification and health monitoring of structural and mechanical systems from changes in their vibration characteristics: A literature review*, LA-13070-MS.

Friswell, M.I. and Mottershead, J.E. (1995), *Finite element model updating in structural dynamics*, Kluwer

Academic Publishers.
Hansen, C. and O'Leary, D.P. (1993), "The use of the l-curve in the regularization of discrete ill-posed problems", *SIAM J. Sci. Comput*., **14**(6), 1487-1503.
Mathworks Inc. (2009), *Matlab user's manual*, Version 7.7; Natick, Massachusetts.
Mordini, A., Savov, K. and Wenzel, H. (2007) "The finite element model updating: a powerful tool for structural health monitoring", *Struct. Eng. Int*., **17**(4), 352-358.
Overschee, P. and DeMoor, B. (1996), *Subspace identification of linear systems: Theory, implementation, applications*, Kluwer Academic Publishers.
Ren, W.X. and Roeck, G.D. (2002), "Structural damage identification using modal data. I: Simulation & verification", *J. Struct. Eng. - ASCE*, **128**(1), 87-95.
Shahverdi, H., Mares, C., Wang. W., Greaves, C.H. and Mottershead, J.E. (2006), "Finite element model updating of large structures by the clustering of parameter sensitivities", *Appl. Mech. Mater*., **5-6**, 85-92.
Stark, P.B. and Parker, R.L. (1995), "Bounded variable least squares: an algorithm and application", *J. Comput. Stat*., **10**, 129-141.
Teughels, A., Maeck, J. and Roeck, G.D. (2002), "Damage assessment by FE model updating using damage functions", *Comput. Struct*., **80**(25), 1869-1879.
Tikhonov, A.V. and Arsenin, V.Y. (1977), *Solution of Ill-posed Problems*, Wiley, New York.
Yu, E., Skolnik, D., Whang D.H. and Wallace, J.W. (2008), "Forced vibration testing of a four-story reinforced concrete building utilizing the nees@UCLA mobile field laboratory", *Earthq. Spectra*, **24**(4), 969-995.
Yu, E., Taciroglu, E. and Wallace, J.W. (2007a), "Parameter identification of framed structures using an improved finite element model updating method - Part I: Formulation & validation", *Earthq. Eng. Struct. D*., **36**(5), 619-639.
Yu, E., Taciroglu, E. and Wallace, J.W. (2007b), "Parameter identification of framed structures using an improved finite element model updating method - Part II: application to experimental data", *Earthq. Eng. Struct. D*., **36**(5), 641-660.
Zhang, Q.W., Chang, C.C. and Chang, T.Y. (2000), "Finite element model updating for structures with parametric constraints", *Earthq. Eng. Struct. D*., **29**(7), 927-944.

CC